

High-Speed Flow Visualization by a Nanosecond Volume Discharge during Shock Wave Diffraction on an Obstacle

I. Mursenkova¹, A. Ivanova², I. Ivanov³, N. Sysoev⁴, A. Karimov⁵

Moscow State University, Faculty of Physics, Russia

¹ ORCID: 0000-0002-7181-4533, murs_i@physics.msu.ru

² ORCID: 0009-0005-5588-5824, militcina.aa18@physics.msu.ru

³ ORCID: 0000-0002-7786-6780, ivanovmai@gmail.com

⁴ ORCID: 0000-0002-1162-7680, nn.sysoev@physics.msu.ru

⁵ ORCID: 0009-0006-4607-3346, karimovzizu@gmail.com

Abstract

We study the spatial structure of nonstationary inhomogeneous supersonic airflows as shock wave diffraction on an obstacle occurs in a shock tube of a rectangular cross section. The Mach numbers of shock waves were 2.7–4.4 at initial air pressures of 10–30 Torr. The supersonic flow in the discharge chamber was visualized by high-speed shadowgraphy and by the registration of radiation of combined volume discharge by photo camera and by ICCD camera. In experiments, a combined volume discharge with a current duration of ~ 500 ns was initiated 40–150 μ s after the initial shock wave have passed an obstacle. It has been established that the radiation of the volume phase of discharge lasts 400–700 ns, and the displacement of the flow during this time does not exceed 0.6 mm. A correlation is established between the spatial distribution of discharge radiation and the low-density local areas determined as a result of two-dimensional Navier-Stokes based numerical simulation of the flow. As visualized by the glow of the discharge, the shape of the shock wave front is in good agreement with the results of shadowgraphy at different stages of diffraction and with the numerical simulation results.

Keywords: shock wave diffraction, supersonic airflow, flow visualization by the discharge radiation, nanosecond combine volume discharge, high-speed shadowgraphy, numerical simulation.

1. Introduction

The use of different types of discharges in supersonic airflows has been studied for the last decades and applied to plasma aerodynamics problems [1-4] that includes the search for optimal discharge modes for active control of flows and shock waves. To visualize flows of transparent media and to obtain quantitative information about the flow classical panoramic methods researchers widely use such methods as direct shadowgraphy, schlieren technique, interferometry [4-6]. These methods are proved to be effective in shock tunnels and wind tunnels with trans- and supersonic flows, where the flow field includes regions with significant changes in density and refractive index of gas. In the last few decades, methods of visualizing the different types of discharge have also been developed to study the structure of gas dynamic flows [1, 7-10]. Such an imaging method is applicable at low gas pressure, when the local radiation intensity of the gas discharge plasma can be related to the local value of the reduced electric field, and hence to the local gas density [11, 12]. It makes it possible to determine the spatial structure of the flow by recording the glow of volumetric discharges. Discharge emission is mainly used to visualize the bow shocks and other structural elements of steady high-speed flows in the vicinity of streamlined objects of various shapes [1, 7, 8]. It should be noted that direct current (DC) discharges significantly change the gas flow due to

Joule heating. Nanosecond discharges (up to 100 ns), which are short compared to gas-dynamic times ($\sim 1 \mu\text{s}$), allow gas-discharge imaging even at high, up to hypersonic, flow velocities [4, 10, 12].

The objective of this work is an experimental study the structure of the airflow after diffraction of a plane shock wave with a Mach number of 2.7-4.4 on a small obstacle in a shock tube of a rectangular cross section. Direct shadowgraphy and nanosecond combined volume discharge visualization were used to study the flow. The discharge was initiated at a pulse voltage of 25 kV, initial air pressure of 10-30 Torr at different times after the shock wave passed an obstacle. Two-dimensional simulation of the flow in the channel during diffraction of a plane shock wave on an obstacle was performed based on the Navier-Stokes equations [13]. The spatial distribution of discharge glow was analyzed taking into account the calculated airflow density fields.

2. Experimental Methods

The study was carried out on a shock tube with a discharge section with an internal cross section of $24 \times 48 \text{ mm}^2$ [4, 12, 14]. The test gas was the air at an initial pressure $p_0 = 10\text{-}30$ Torr. After the rupture of the diaphragm, a flow with a plane shock wave is formed in the shock tube channel, followed by a homogeneous co-current flow [10, 15, 16]. The shockwave front is a plane perpendicular to the channel walls. The Mach numbers of the shock waves in the experiments were $M=2.7\text{-}4.4$. Piezoelectric pressure sensors were used to measure the shockwave velocity, to synchronize the processes in the experiments, and to generate a signal to start the discharge.

On the lower wall of the working section, at a distance of 30 mm from the beginning of the discharge volume, there was a small parallelepiped-shaped obstacle of a size of $6 \times 2 \times 48 \text{ mm}^3$ ($x \times y \times z$) (Fig. 1). The discharge volume was of 100 mm length along the direction of shock wave propagation. The end of electrodes was taken as the zero coordinate x . The delay time on the generator was set so that at the moment of discharge the shock wave was within the discharge gap or beyond it at a certain distance from the obstacle.

Shadowgraphy of the flow was performed through the quartz sidewalls of the working section. A continuous laser with a wavelength of 532 nm was used as a light source. The optical system was generating a parallel beam of light ~ 40 mm wide to pass through the flat-parallel quartz glasses of the discharge chamber and uniformly probe the field-of-view [4]. A high-speed camera was used to record the shadowgraphy images with a frequency of 150 000 fps. The photo camera records the integral discharge glow and the exposure time corresponds to the discharge radiation time. ICCD camera K011 [17] was used to record the discharge emission with nanosecond resolution. The camera operates in the nine-frame recording mode with an exposure time of 100 ns, and a delay time between frames from 100 to 300 ns.

During diffraction on a rectangular obstacle, the upper part of the plane shock wave front continues to move straight ahead, while the lower part diffracts and slows down [15, 18]. As shown by numerical simulations [18, 19], at the initial stage of diffraction, the shock wave front acquires a curved profile because it starts to move not only in the horizontal direction but also in the vertical direction, first along the front surface of the obstacle and then along the rear surface. Figure 1, *b* shows shadowgraphy images with the shock wave front before interaction with the obstacle (4), at the beginning of diffraction (5), and as it moves away from the obstacle (6, 7). High-speed shadowgraphy revealed the peculiarities of the motion of the diffracted shock wave. In the shadowgraphy images of Fig. 1, *b* (6, 7), there is an oblique shock behind the front, which distorts the front of the moving shock wave. As it moves away from the obstacle in a homogeneous medium, the curvature of the front decreases [15]. In the experiments, the shock wave front regains a flat shape at a distance $x > -10$ mm. The formation of a quasi-stationary flow after the diffraction of the shock wave by the obstacle occurs within 100–200 μs , as shown using high-speed imaging [19].

A pulsed combined volume discharge was initiated in the working section at a given time [14, 18]. Plasma sheets (surface sliding discharges) of $30 \times 100 \text{ mm}^2$ area on the upper and lower walls of the discharge chamber provided preionization of the gas volume [14]. At a pulse voltage of 25 kV, the discharge current was of $\sim 1 \text{ kA}$ at $\sim 500 \text{ ns}$ duration. A pulse generator synchronized with the signal from the piezoelectric pressure sensor in the shock tube channel during passage of the shock wave triggered the discharge. In the experiments performed, the discharge occurs when the shock wave passed a distance of 24 to 104 mm after the diffraction, i.e., at a distance of $-40 \text{ mm} < x < +60 \text{ mm}$ relative to the end of the discharge volume (Fig. 1).

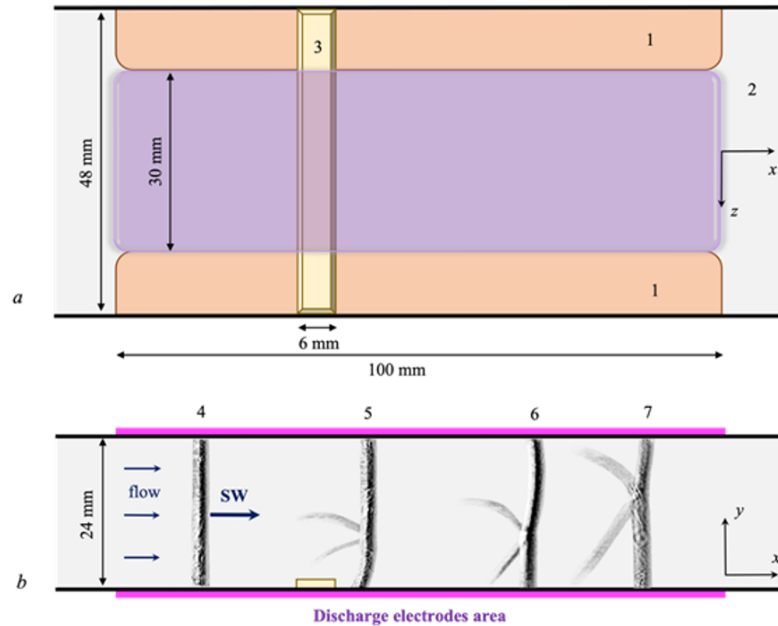


Fig. 1. Scheme of discharge volume and flow in the working section: a) top view, b) side view; 1 - surface sliding discharge electrodes, 2 - dielectric; 3 - obstacle; 4-7 - shadowgraph images of the shock wave before diffraction (4) and after diffraction (5-7) at times 6, 35, 51 μs at $x = -58; -31; -15 \text{ mm}$, respectively. ($t = 0$ when the shock wave hits the front edge of the obstacle). The Mach number of the shock wave is $M = 2.80$, and the initial pressure is $p_0 = 18 \text{ Torr}$. Arrows indicate the direction of shock wave and the direction of co-current flow.

3. Numerical Simulations of Shock wave Diffraction

Numerical simulation was carried out to study the dynamics of a shock wave in a two-dimensional straight channel with a rectangular obstacle. The system of Navier–Stokes equations was used as a mathematical model for the supersonic flow in a channel and the shock wave diffraction on an obstacle [13, 19]. The system describes the flow of a viscous, compressible gas taking into account the effects of turbulence using a modified $k-\varepsilon$ turbulence model [13]. A model of heat-conducting, thermodynamically perfect gas (air) with a constant isentropic index ($\gamma = 1.4$) and Prandtl number $Pr = 0.72$ was used. The temperature dependence of the viscosity coefficient is described by the Sutherland formula. The numerical algorithm based on the second-order finite-volume scheme [13] is conservative and monotonic and has the second order in space and time. To approximate time derivatives, the Runge–Kutta method of the second order is used.

The computational algorithm was implemented to use a two-dimensional, nonuniform, structured finite-volume computational grid with quadrangular cells. The computational grid has dimensions of 600×100 cells and is refined in the direction of the solid walls, so that the first nodal point of the grid from the wall is at a distance $y = 0.2-0.5$ from the wall. In this case, the size of the first cell near wall is no more than 0.000058 m . The upper and lower boundaries of the computational region and the boundaries of the obstacle are solid walls on

which the no slip condition is set. The parameters of shock wave and airflow were set in accordance with the experimental conditions.

4. Results and Discussion

The front of a shock wave moving in a channel is a plane that separates the low-pressure state of air (in front of the shock wave) and the high-pressure state (behind the shock wave). When the shock wave is inside the discharge volume at the moment of applying the pulse voltage, the magnitude of the reduced electric field E/N in front of a shock wave is greater than behind it (E – electric field strength, N – molecule concentration). This parameter determines the ionization rate of gas molecules [11] and the magnitude of electron concentration. The increased concentration of electrons in the low-pressure region leads to the volume discharge current in front of the shock wave, so the discharge glow is localized in front of the shock wave [14, 18].

The spatial distribution of discharge glow in the photo images at different shock wave positions (Fig. 2) shows the area of volume discharge current with a sharp glow boundary on the left. The pulsed breakdown is of volumetric character, and the discharge glow clearly visualizes the curved front of the diffracted shock wave (Fig. 1). The distribution of discharge glow allows for accurate determination of the position and shape of the shock wave front after diffraction.

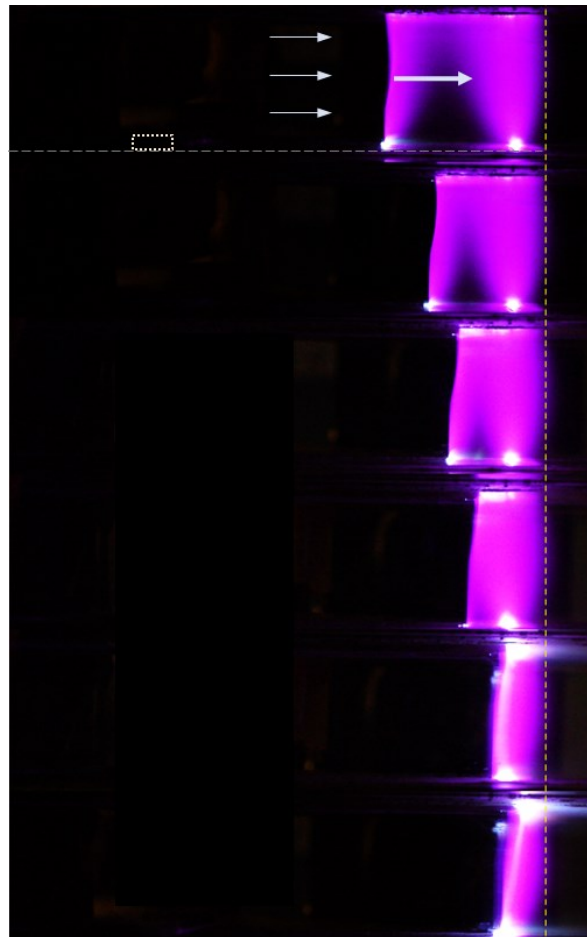


Fig. 2. Sequence of discharge photo images with a diffracted shock wave at different distances from the obstacle. The Mach number of the shock wave is $M = 4.30 \pm 0.06$, and the initial pressure is $p_0 = 10$ Torr. The end of the discharge volume is indicated with a dashed vertical line. Arrows indicate the direction of shock wave and the direction of flow. The obstacle is shown on the top image.

Fig. 3 shows a discharge photo image (a) and the corresponding sequence of frames captured by ICCD camera (c), which show the emission of a plasma volume with a length of 6 mm. In Fig. 3, *b* is an enlarged fragment, which is highlighted by a dashed line in Fig. 3, *c*. On the first electron-optical frame, a bright stage of volume discharge glow is observed for 100 ns, corresponding to the current flow in the region limited by the curved front of the diffracted shock wave. On the second and third frames, the volume discharge phase fades. A fading afterglow of surface discharges on the lower and upper walls is observed on the following frames. As a result, the total duration of the volume phase of the discharge emission in the experiments was 400-700 ns. The photo images of the combined volume discharge in Fig. 2, 3, *a* are time-integrated images of the glow, and the exposure time corresponds to the discharge emission time. Since the displacement of the shock wave front during the exposure time does not exceed 0.6 mm, the photo registration of the glow provides almost instantaneous visualization of the shock wave front.

It should be noted that the spectral sensitivity range of the digital camera and the ICCD camera corresponds to the visible and part of the infrared radiation range (380-800 nm), while the main part of the spectrum of pulsed discharges in air is in the ultraviolet region, corresponding to bands of the second positive system of nitrogen with wavelengths of 280-500 nm [4, 10].

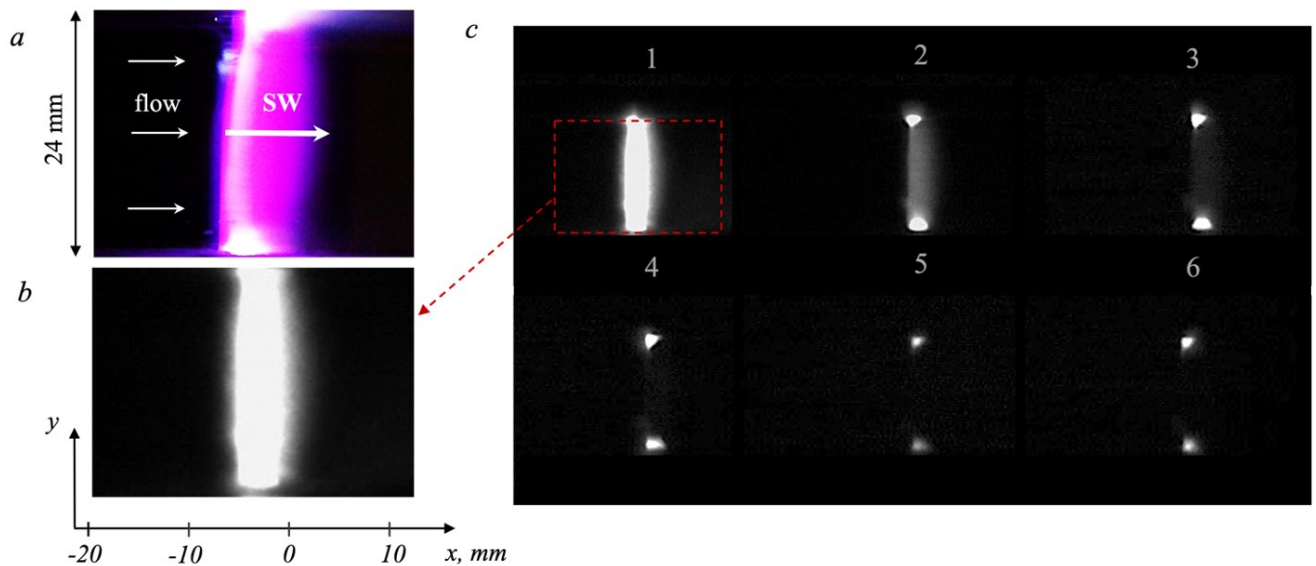


Fig. 3. (a) Discharge photo image; (b) the first frame and (c) a series of frames captured by ICCD camera with an exposure time of 100 ns, with a pause of 100 ns between frames. The frame numbers are indicated. The discharge was initiated 47 μ s after the shock wave passed the obstacle ($M = 4.36$, $p_0 = 10$ Torr).

Digital processing of the images of the discharge glow have allowed us to find out that the distribution of the glow makes it possible to determine with great accuracy the position and shape of the shock wave front after diffraction. Fig. 4 shows a shadowgraph image of the shock wave front that has moved 47 mm away from the obstacle, a discharge photo image, and ICCD images with an exposure time of 100 ns, showing the emission of a plasma volume with a length of about 12 mm. It is evident that the discharge glow (Fig. 4, *b-g*) clearly visualizes the curved front of the diffracted shock wave and corresponds well to the shadowgraph image (Fig. 4, *a*).

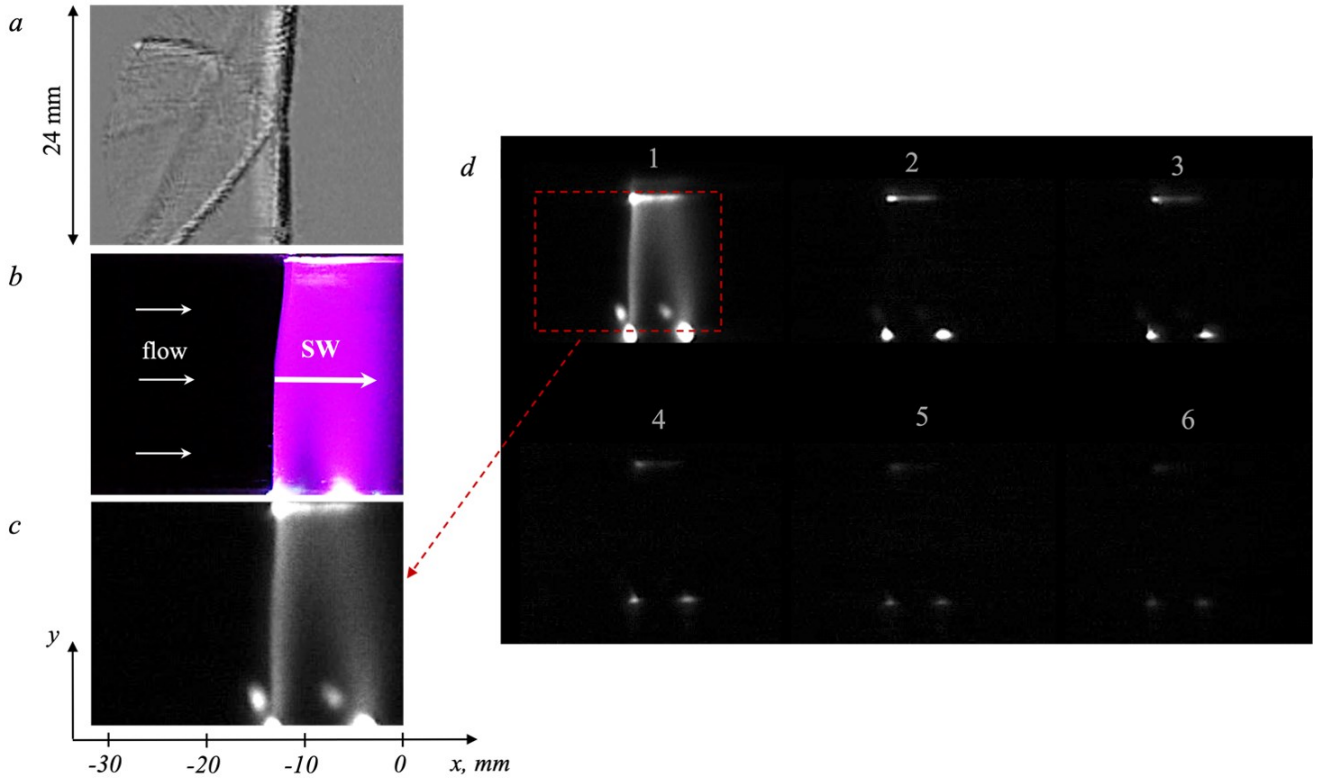


Fig. 4. (a) Shadowgraph image of the shock wave ($M = 3.0$, $p_0 = 25$ Torr), $1 \mu\text{s}$ exposure time; (b) discharge glow photo image; (c) the first frame and (d) a series of frames captured by an electrooptical camera with an exposure time of 100 ns , with a pause of 200 ns between frames. The discharge was initiated $52 \mu\text{s}$ after the shock wave passed the obstacle ($M = 3.15$, $p_0 = 25$ Torr).

Numerical simulation of the flow in the channel after the diffraction of a plane shock wave on a rectangular obstacle was carried out for a Mach number of the initial shock wave of 3.20 . The shock wave and gas flow were propagating from left to right in the computational domain (Fig. 5). On the left boundary, the supersonic inlet flow is set, and on the right outlet boundary, the condition of non-reflection is set. The flow density fields are shown in Fig. 5 in the time interval $7\text{-}130 \mu\text{s}$ after the diffraction (from top to bottom). It can be seen how the plane shock wave passes near the obstacle and, as a result of diffraction, compression and rarefaction waves are formed. At the initial stage of diffraction, the upper part of the initial shock wave moves to the right, and the diffracted part moves to the left of the obstacle. In the next stage, the non-stationary stage includes the inclined shock wave forming behind the bottom of the obstacle and disturbances in front of the obstacle, where the head shock wave is formed. At a distance of $\sim 5 \text{ mm}$ behind the bottom of the obstacle, a rarefaction wave is generated, which interacts with the front of the initial shock wave, causing it to bend ($45, 58 \mu\text{s}$). As the distance from the obstacle increases, the curvature of the moving shock wave front decreases ($83 \mu\text{s}$). A non-stationary inhomogeneous supersonic flow is formed behind the front ($83, 130 \mu\text{s}$). The unsteady supersonic flow lasts up to $200 \mu\text{s}$, as shown using high-speed imaging [4, 19]. When the shock wave is outside the discharge volume at the moment of discharge initiation a complex spatial distribution of discharge radiation is observed (Fig. 6).

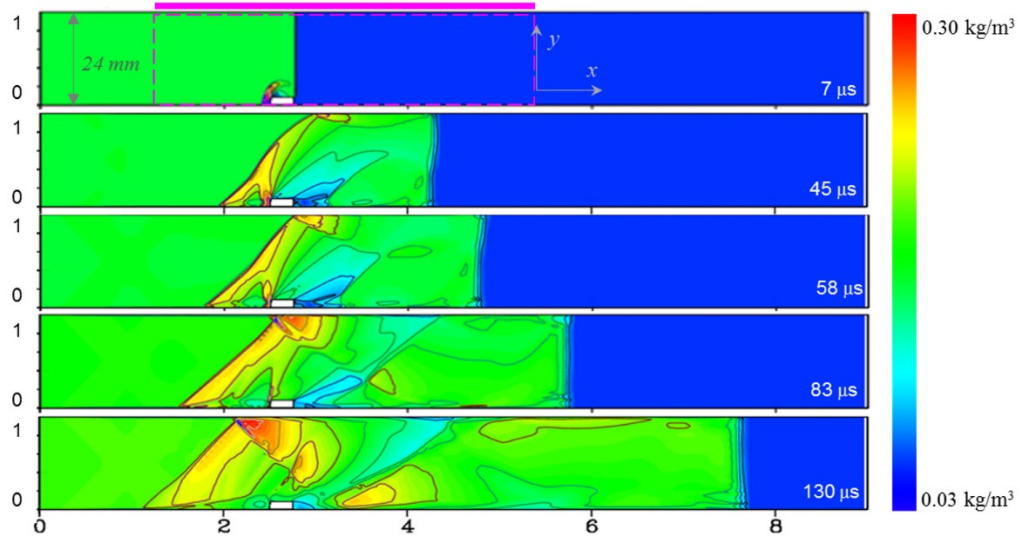


Fig. 5. Calculated density fields after the diffraction of a plane shock wave by an obstacle. Mach number of shock wave is 3.20, initial air pressure is 18 Torr and initial density is 0.03 kg/m^3 . The time is indicated from the moment of contact of the shock wave with the front edge of the obstacle. The linear scale is normalized to 24 mm. The dotted rectangle on the top image shows the area of the pulsed electric field.

A photo of the discharge glow with a shock wave 10 mm beyond the discharge volume is shown in Fig. 6, *a*. Discharge glow is observed ahead of the front, which is associated with the presence of an electric field outside the electrodes. Behind the front, in the supersonic flow, discharge emission is observed in the volume behind the obstacle, from the bottom wall upwards, and near the top wall as well as near the bottom wall ahead of the obstacle. The distribution of discharge glow correlates well with the density distribution in the air flow (Fig. 5, 83 μs). Areas of reduced density at this diffraction stage are located behind the obstacle at the bottom, and further upwards to the wall, where surface discharge glow is clearly visible. As the shock wave moves further away from the obstacle, the density distribution in the flow changes (Fig. 6, *b*). An inclined rarefaction wave is formed behind the obstacle, and the area of reduced density expands (Fig. 5, 130 μs). When the discharge is initiated at this stage, the discharge glow is concentrated only behind the obstacle and visualizes the area of low density with a sharp right boundary (Fig. 6, *b*). The ICCD imaging showed that the duration of the volume phase of the discharge glow is no more than 300 ns. The flow displacement during this time does not exceed 0.3 mm, and the photo registration of the discharge glow provides almost instantaneous gas discharge visualization of the shock wave structure of the supersonic flow.

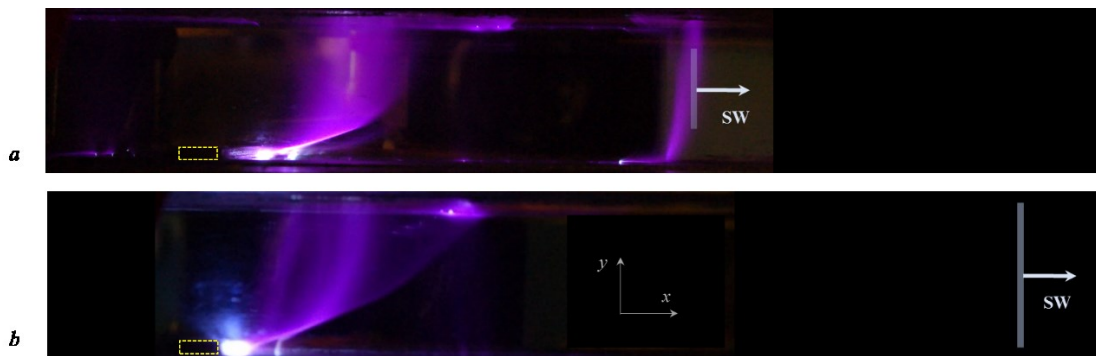


Fig. 6. Photo images of the discharge with the shock wave located outside the discharge volume: a) $M = 4.20$, $p_0 = 10 \text{ Torr}$, $x = +10 \text{ mm}$, b) $M = 3.25$, $p_0 = 25 \text{ Torr}$, $x = +50 \text{ mm}$. Arrows indicate the direction of diffracted shock wave. The dotted rectangle shows the obstacle on the bottom.

5. Conclusion

Experimental investigation of inhomogeneous supersonic flow in a channel during the diffraction of shock wave on an obstacle was carried out by registration the emission of a combined volume discharge of nanosecond duration and by direct shadowgraphy. A volume discharge with a duration of ~500 ns was initiated at different stages of shock wave diffraction by an obstacle. Mach number of shock wave were 2.7-4.4. It was shown that the distribution of volume discharge glow of a duration of 400–700 ns accurately visualizes the shape of the shock wave front, which is curved as a result of diffraction, and is in good agreement with the shadowgraph images of the flow. Considering numerical calculations of the flow, an analysis of the distribution of discharge glow during its development in the presence of a diffracted shock wave inside and outside the discharge volume was carried out. It was shown that photo registration of the discharge glow allows for visualization of the structure of the non-stationary supersonic flow at different stages. The investigated discharge type is a good tool for gas discharge visualization of supersonic airflow in a profiled channel and, with the use of multi-angle imaging, can provide information about the three-dimensional structure of the flow.

The work was carried out within the framework of the Interdisciplinary Scientific and Educational School of Moscow State University “Photonic and Quantum Technologies: Digital Medicine”. Project No 001986 «Plasma technologies in interdisciplinary applications: plasma aerodynamics and microelectronics».

References

1. **V.P. Alfeyorov, L.M. Dmitriev.** Electric-discharge in a gas-flow in the presence of density gradients // High Temperature. 1986. Vol. 23. N. 4. P. 539-543.
2. **V.G. Gromov, A.P. Ershov, V.A. Levin & V.M. Shibkov.** Transverse electric discharges in supersonic air flows: Simulation of the effects influencing the heating of gas in discharge channel. // High Temperature. 2006. Vol. 44. N 2. P. 178–188. DOI: <https://doi.org/10.1007/s10740-006-0022-2>
3. **A.Yu. Starikovskiy, N.L. Aleksandrov.** Gasdynamic Flow Control by Ultrafast Local Heating in a Strongly Nonequilibrium Pulsed Plasma // Plasma Physics Reports. 2021. V. 47. P. 148. <https://doi.org/10.1134/S1063780X21020069>
4. **I.V. Mursenkova, Yu. Liao, P.Yu Ulanov, L. Shi.** High-Speed Shadowgraphy of the Interaction of an Oblique Shock Wave in a Channel with a Surface Sliding Discharge // Scientific Visualization. 2021. Vol. 13. N 3. P. 47-57. DOI: 10.26583/sv.13.3.05
5. **G.S. Settles, M.J. Hargather** A review of recent developments in schlieren and shadowgraph techniques // Measurement Science and Technology. 2017. V. 28. N 4. 042001. DOI 10.1088/1361-6501/aa5748
6. **I.A. Znamenskaya.** Methods for Panoramic Visualization and Digital Analysis of Thermophysical Flow Fields. A Review // Scientific Visualization, 2021. Vol. 13. N 3. P. 125 – 158. DOI: 10.26583/sv.13.3.13
7. **G. Jagadeesh, Rao B.R. Srinivasa, K. Nagashetty, N.M. Reddy, K.P.J. Reddy.** Electrical discharge technique for three-dimensional flow field visualisation in hypersonic shock tunnel // J. Flow Visualisation and Image Processing. 1997. V. 4. N^o1. P. 51-57. DOI: 10.1615/JFlowVisImageProc.v4.i1.50
8. **M. Nishio, Sh. Sezaki and H. Nakamura.** Visualization of Flow Structure Around a Hypersonic Re-entry Capsule Using the Electrical Discharge Method // Journal of Visualization. 2004. V. 7, N^o 2. P. 151-158. <https://doi.org/10.1007/BF03181588>
9. **V. Lago, R. Jousot and J.-D. Parisse.** Influence of the ionization rate of a plasma discharge applied to the modification of a supersonic low Reynolds number flow field around a cylinder // Journal of Physics D: Applied Physics, 2014. V 47. N 12. DOI:10.1088/0022-3727/47/12/125202

10. **Mursenkova, A. Sazonov, Yu. Liao, I. Ivanov.** Visualization of the interaction region of an oblique shock wave with a boundary layer by the radiation of a nanosecond surface sliding discharge // *Scientific Visualization*, 2019. Vol. 13. N 3. P. 76 – 87. DOI: 10.26583/sv.11.3.07
11. **Raizer Yu. P.** *Gas Discharge Physics*. Berlin: Springer, 1991
12. **W. Jiang, H. Qiu, Y. Yang, Y. Shi, J. Wang, J. Li, Z. Long, and C. Mao.** High frequency AC electric glow discharge visualization technology and application in big diameter hypersonic low-density wind tunnel // *Adv. Aerodyn.* 2021. V. 3, N 1. 14. DOI:10.1186/s42774-021-00067-w
13. **Glushko G.S., Ivanov I.E., Kryukov I.A.** Computational method for turbulent supersonic flows. *Math. Model. Comput. Simul.*, 2010. N 2. P. 407–422. DOI:10.1134/S2070048210040010
14. **N.O. Arkhipov, I.A. Znamenskaya, I.V. Mursenkova, I.Yu. Ostapenko, N.N. Sysoev.** Development of nanosecond combined volume discharge with plasma electrodes in an air flow // *Moscow University Physics Bulletin*. 2014. V. 69, N 1. P. 96. <https://doi.org/10.3103/S0027134914010020>
15. **Shugaev F.V. and Shtemenko L.S.** *Propagation and Reflection of Shock Waves*. 1998. World Sciences, Series on Advanced in Mathematics for Applied Sciences, vol.49 Singapore. 260 p. <https://doi.org/10.1142/3358>
16. **I.A. Znamenskaya, I.V. Mursenkova, N.N. Sysoev.** Experimental investigation of shock-wave processes in the pulsed ionization of the surface of a shock-tube channel // *Journal of Engineering Physics and Thermophysics*. 2011. Vol. 84, no. 1. P. 33–38. DOI:10.1007/s10891-011-0453-4
17. <https://www.vniiofi.ru/depart/r5/k011.html>
18. **I.A. Znamenskaya, D.I. Dolbnya, I.E. Ivanov, T.A. Kuli-zade, N.N. Sysoev.** Pulse volume discharge behind shock wave in channel flow with obstacle // *Acta Astronautica*. 2022. Vol. 195. P. 493–501. <https://doi.org/10.1016/j.actaastro.2022.03.031>
19. **I.V. Mursenkova, I.E. Ivanov, Yu. Liao, I.A. Kryukov.** Experimental and Numerical Investigation of a Surface Sliding Discharge in a Supersonic Flow with an Oblique Shock Wave // *Energies*, MDPI, 2022. Vol. 15. No 6. 2189. <https://doi.org/10.3390/en15062189>